Journal of Vacuum Science Technology A



# Growth of $(Sm_xGa_{1-x})_2O_3$ by Molecular Beam Epitaxy

Anthony D. Stewart[1], Brent P. Gila[2], Cammy R. Abernathy[2] and S.J. Pearton[2*]

Department of Physics, Southern University and A&M College, Baton Rouge, LA 70813

Department of Materials Science and Engineering, University of Florida, Gainesville, FL 32611 USA

## Abstract

The $(Sm_xGa_{1-x})_2O_3$ alloy system is a potential new dielectric for compound semiconductors such as GaAs. Using molecular beam epitaxy under metal-modulated growth conditions, we grew the binary oxide, $Sm_2O_3$, at two substrate temperatures (100 and 500°C) and optimized the structural, morphological and electrical properties of the films. Decreasing the Sm cell temperature suppressed formation of the monoclinic phase and promoted the growth of the cubic phase. Next, the ternary oxide, $(Sm_xGa_{1-x})_2O_3$, was deposited to investigate the effects of Ga incorporation. Optimization experiments were used to determine the effects of substrate temperature and samarium cell temperature (i.e. growth rate) on film stoichiometry, phase distribution, and microstructure in these films. Films grown at 500°C showed significant surface roughness and the presence of multiple crystalline phases. Since all of the Sm- based oxides (i.e. samarium oxide with and without gallium) were found to have unbonded Sm metal, annealing experiments were carried out in oxygen and forming gas to determine the effects of annealing on film stoichiometry. The motivation behind annealing in forming gas was to see if this commonly used technique for reducing interface densities could improve the film quality. GaAs metal-oxide-semiconductor diodes with $(Sm_xGa_{1-x})_2O_3$ showed breakdown fields at 1 mA/cm$^2$ of 4.35 MV/cm, which decreased with increasing Sm unbonded metal content in the films.

*Corresponding author, email spear@mse.ufl.edu

## Introduction

There remains significant interest in advanced compound semiconductor metal oxide semiconductor field effect transistor (MOSFETs) and the related development of gate dielectrics to reduce leakage current, passivate surface traps, and provide electrical isolation between devices [1-14]. The use of InGaAs, InAs, GaSb or GaAs as channel materials for MOSFETs with high speed and low power due to their higher electron mobility are hampered by the lack of a stable high-quality native oxide [15-27]. Typically, these III-V MOS devices cannot reach their full potential because of poor oxide/semiconductor interfacial properties that pin the Fermi-level at the semiconductor surface [2,4,5,10]. Despite of all the advantages these have as channel materials for MOSFET technology compared to Si, there is still an urgent need for a technology capable of forming insulating layers on them with dielectric and interface properties comparable to the Si-$SiO_2$ system [12-14]. Especially when using high-k gate dielectrics, Coulomb scattering and interface-roughness scattering significantly reduce the carrier mobility. A suitable gate dielectric material must satisfy two requirements [4,22-25]: (1) the interface between the semiconductor and the gate dielectric must have a low interface state density ($D_{it}$) to prevent the Fermi level from being pinned; and (2) the gate dielectric must have a high breakdown field to allow a gate voltage to be established. Samarium oxide ($Sm_2O_3$) and samarium gallium oxide $(Sm_xGa_{1-x})_2O_3$ are potential candidate dielectric materials for III-V MOSFET technology [28-32]. $Sm_2O_3$ has a high κ (14-16), high breakdown electric field (5-7 MV/cm), large bandgap (4.33 eV) [28-32], large conduction offset with GaAs [33], and low hygroscopic characteristics [29,30]. $Sm_2O_3$ has a bixbyite crystal structure which is composed of two interpenetrating face-centered cubic. The lattice parameter of $Sm_2O_3$ is 5.32 nm representing a lattice mismatch of 3.3% with the zinc blende cubic structure of GaAs (lattice parameter 5.65 nm).

In this work, growth of thin (20nm-50nm) samarium oxide and samarium gallium oxide layers on GaAs substrates via plasma-assisted molecular beam epitaxy (MBE) was performed using

two growth temperatures (100ºC and 500ºC) in an attempt to affect the crystallinity (amorphous vs. crystalline) of the oxide and samarium cell temperatures that were typically 570°C. There was residual Sm metal in the films, which decreased with decreasing Sm cell temperature, but was relatively independent of substrate temperature. The stoichiometry of the oxides was found to be independent of substrate temperature but increased in oxygen to metal ratio as the Sm cell temperature was decreased, as low as 510°C. Decreasing the Sm cell temperature also suppressed the formation of the monoclinic phase and promoted the growth of the cubic phase. Films grown at higher (500ºC) temperature showed the presence of a crystalline interface, but relatively high surface roughness and the presence of multiple crystalline phases. MOS diodes showed breakdown fields at 1 mA/cm$^2$ up to 4.35 MV/cm, which was found to decrease with increasing Sm free metal content in the films. Post-growth annealing under an oxygen plasma of films grown at higher temperatures resulted in an increase in the oxygen to metal ratio but no change in the crystalline phase distribution.

**Experimental**

A Riber 2300 MBE system was used for all the oxide growths [(2)]. The growth chamber was evacuated to 1-5x10$^{-9}$ torr using an Oxford Cryo-Torr 8 cryopump. Pure Sm and Ga were used as the metal sources. The temperature of the Knudsen cells was controlled by a FICS 10 controller that adjusts the power output of an external power supply. An MDP21 radio frequency (rf) source from Oxford Applied Research was used as the oxygen source and operated at a frequency of 13.56 MHz with a forward power of 300W and reflected power of 2-3W. Oxygen (99.995%) was supplied to the plasma head using a high purity $O_2$ mass flow controller (MFC) that had a 3 sccm full scale range. The substrate temperature was measured using a backside thermocouple, while the GaAs substrate surfaces were cleaned by ex-situ etching with a solution of $H_3PO_4$:$H_2O$ (3:80) for 90 seconds [(34)] and then an in-situ exposure time of 20-30 minutes with a hydrogen plasma under vacuum.

The films were characterized by x-ray photoelectron spectroscopy (XPS) using a Perkin-Elmer PHI 5100 ESCA system, auger electron spectroscopy (AES) using a Perkin Elmer 6600 system fitted with an Ar sputter gun allowing compositional depth profiling, x-ray diffraction (XRD) performed using a Phillips APD 3720 diffractometer with a copper (Cu) x-ray source, atomic force microscopy (AFM) measurements done using a Dimension 3100 system and reflection high energy electron diffraction (RHEED) using a Staib electron gun operating at 15 kV. Following oxide deposition, MOS capacitors were fabricated using a standard shadow mask process. All electrical measurements were conducted with a Signatone S-1160 Series General Purpose Analytical Probe Station. Current-voltage (I-V) measurements were performed with an Agilent 4155C Semiconductor Parameter Analyzer. Capacitance-voltage (C-V) measurements were performed on an Agilent 4284A 20Hz-1MHz Precision LCR meter connected to a Lab View based PC. Breakdown voltages were extracted from the I-V plot at a current density of 1mA/cm$^2$. The extracted voltages were then divided by the dielectric film thickness to determine the forward and reverse breakdown voltages. The data from the C-V curve was used to determine the interface state density, flat band voltage shift, and dielectric constant. The $D_{it}$ value and capacitance-voltage behavior of MOS diodes consisting of a bi-layer structure of Pt (20 nm)/Au (80 nm) contacts on the dielectric were used to evaluate the relationship between growth conditions and interfacial quality [35-38]. Preliminary work on developing $SmO_2$ has been published previously [33,38].

**Results and Discussion**

The initial aim was optimization of the growth conditions and their effects on stoichiometry, phase distribution and microstructure. Since the surface properties of the semiconductor will largely affect the properties of the deposited film, initial experiments focused on deposition of the binary oxide, $Sm_2O_3$, at two substrate temperatures, followed by growth of the ternary oxide, $(Sm_xGa_{1-x})_2O_3$ to investigate the effects of Ga incorporation.

**(a) Growth at Low Substrate Temperature**

The data from the next two sections is shown in the Supplemental file S to avoid making the main manuscript overly long-See supplementary material at [URL will be inserted by AIP Publishing] for a summary of XRD, RMS surface roughness and XPS of film composition. XRD measurements of $Sm_2O_3$ grown on GaAs at a substrate temperature of 100ºC showed an amorphous nature of the film verified by RHEED measurements, with peaks at 32.15º and 66.53º associated with GaAs (200) and the GaAs (400) of the cubic phase (Figure S1). XRD scans of films grown at 100ºC showed no peaks related to the oxide film. The RMS roughness value was measured at 1.4 nm (Figure S2). XPS measurements confirmed the presence of Sm free metal in the film, with a broad peak located at 1082.5 eV representing the Sm free metal peak and a more dominant peak associated with Sm bonded to O (Figure S3). The breakdown field strength was measured at 3.96 MV/cm (Figure S4).

**(b) Growth at High Substrate Temperature**

XRD measurements of $Sm_2O_3$ grown on GaAs at a substrate temperature of 500ºC showed a crystalline nature of the film verified by RHEED measurements. The RHEED images remained streaky for the duration of growth (Figure S5). XRD measurements showed a broad peak at 29.95º attributed to the $Sm_2O_3$ (321) of the cubic phase and a peak at 44.15º associated with $Sm_2O_3$ (403) of the monoclinic phase (Figure S6). There was also a small shoulder at 28.33º associated with $Sm_2O_3$ (222) of the cubic phase. Peaks at 32.15º and 66.53º are associated with GaAs (200) and the GaAs (400) of the cubic phase. AFM measurements revealed a smooth film surface with a RMS roughness value of 0.631 nm (Figure S7). XPS measurements confirmed the presence of Sm free metal in the film. The small broad peak located at 1078.9 eV represents the Sm free metal peak and the peak at 1082.3 represent Sm bonded to O (Figure S8). The breakdown field strength was measured at 3.38

MV/cm (Figure S9). The C-V characteristics from diodes fabricated on these films showed a very small change in capacitance when swept from depletion to accumulation.

**(c) Growth and Characterization of Ternary Oxides Grown at 100ºC**

The degree of crystallinity was investigated to determine a set of growth conditions for growing a thermally and environmentally stable oxide film. A low growth temperature was chosen to promote the growth of an amorphous or fine-grained poly-crystalline dielectric film which from previous work has been shown to enhance I-V performance [2,39]. A low growth temperature is also ideally suited for these experiments due to the delicate nature of the clean GaAs surface. After the substrate was cleaned, the sample was rotated out of the growth position. The $H_2$ plasma was discharged, the $O_2$ plasma ignited and the sample was then rotated back into the growth position. The samarium cell shutter and the $O_2$ plasma shutter were opened simultaneously to initiate oxide growth. This growth procedure was also used for the oxides grown at 300ºC and 500ºC.

Powder XRD measurements of films grown at 100ºC with a $T_{Sm}$ of 550ºC revealed no evidence of peaks associated with crystalline oxides, suggesting that the films are amorphous or very fine grained polycrystalline. Peaks located at 31.9º and 66.3º are associated with the GaAs (200) and GaAs (400). The peak at 59.1º could not be identified with JCPDS files, but it consistently shows up in scans of the GaAs substrate. This peak could be attributed to an artifact due to the polychromatic of the x-ray source used in the powder system. The growth rate was 12.9 Å/sec. The RHEED pattern immediately disappeared at the onset of oxide growth and never returns, also suggesting an amorphous film. TEM micrographs confirmed the presence of an amorphous interfacial region of approximately 65 Å (Figure 1). The surface was smooth with an RMS roughness measured by AFM of 0.37 nm. An AES survey scan of the oxide surface revealed Sm, Ga, O concentrations of 45.1%, 4.0%, and 50.9% respectively. A depth profile showed that the Ga concentration remained constant throughout the thickness of the film, except for a sharp increase in the O and Ga concentration due to

the presence of gallium oxide at the interface (Figure 2(a)). The cycle interval was 0.20 min/cycle. To confirm that the Ga was being incorporated from the source beam and not from the GaAs substrate, a depth profile was conducted on a silicon substrate mounted on the same molybdenum block during the same growth run. This sample also showed the presence of Ga throughout the deposited film.

Films grown at 100ºC showed a breakdown field strength as high as 3.63 MV/cm. The C- V characteristics, shown in Figure 2(b), clearly showed accumulation in the forward direction, but full depletion in the reverse direction was not reached before reverse breakdown occurred. The gate voltage was swept from depletion to accumulation.

To investigate the effect of Sm cell temperature, films were grown using Sm cell temperatures ranging from 510ºC to 570ºC. As expected, the growth rate increased with increasing cell temperature, Figure 3(a). AES indicated that the Ga composition ranges from 1.3% to just over 10%. X-ray photoelectron spectroscopy (XPS) of the deposited films showed evidence of residual Sm metal in the films which was highest at the highest Sm cell temperature (Table 1). The AFM root mean square roughness is also given in the Table and are accurate to two significant figures. The reason for the presence of residual metal is most likely due to the reduced oxygen to metal ratio present during growth given that the Sm flux is increasing with increasing cell temperature. As one would expect, the breakdown field was lowest in the film with the largest amount of free metal, as shown in Figure 3(b). The layer grown at a $T_{Sm}$ = 550ºC showed the highest oxygen to metal ratio, the lowest RMS surface roughness (Figure 4) and had a good breakdown field. Subsequent growths were performed using this cell temperature.

**(d) Growth and Characterization of Ternary Oxides Grown at Higher Substrate Temperatures**

Films grown at 300ºC using the same procedure as in the previous section showed streaky-dashed RHEED patterns which appeared around five minutes into the oxide growth corresponding to thickness of ~ 5.4 nm (i.e. growth rate of 1.08 nm/sec). The initial streaky RHEED pattern of the GaAs substrate disappeared after one minute of oxide growth. After thirty minutes of oxide growth the RHEED pattern showed a mixture of arcs and lines suggesting the polycrystalline nature of the film at the end of growth. The background pressure in the chamber was $5x10^{-6}$ Torr. Powder XRD measurements revealed a textured morphology, as shown in Figure 5(a). Peaks at 28.9º, 42.2º and 52.3º are associated with the cubic phase of $Sm_2O_3$ (222), $Sm_2O_3$ (134), and $Sm_2O_3$ (026) orientations, respectively. Peaks located at 47.3º and 54.8º are associated with the monoclinic phase of the $Sm_2O_3$ (602) and $Sm_2O_3$ (514) orientations. The remaining peaks in the spectrum are attributed the GaAs substrate. An Auger survey scan confirmed the Sm, Ga, and O concentrations of 49.7%, 6.5%, and 43.9% respectively. Gallium was also detected throughout the thickness of the oxide with a sharp increase in Ga concentration occurring around 25 cycles into the depth profile with a cycle interval of 0.20 min/cycle. XPS analysis of the films showed an Oxygen to Sm metal ratio roughly comparable to that obtained in films grown at 100ºC (Table 2). The film showed an RMS roughness of 0.7 nm. Electrical characterization of diodes fabricated from the material showed a breakdown field strength was 3.68 MV/cm, and poor C-V behavior with no indication of accumulation or complete depletion before breakdown occurred.

Films grown at 500ºC showed a bright streaky RHEED pattern with thick diffuse lines after twelve seconds of oxide growth. As the growth proceeds, the lines became faint and arcs began to appear. Sm cell temperatures of 510ºC and 550ºC were investigated. XRD analysis indicated that the 550ºC cell temperature enhanced the formation of the cubic phase (Figures 5(b) and (c). Therefore, a 550ºC cell temperature was used for subsequent growths.

As compared to the films grown at 300ºC with the same Sm cell temperature, the crystal quality of the cubic phase was enhanced based on an increase in intensity of the peak located at 30.1º (Figure 5(c)). This peak is labeled C and shows up only on the XRD scan of $(Sm_xGa_{1-x})_2O_3$ grown at a substrate temperature of 500ºC and a Sm cell temperature of 550ºC (green curve in Figure 5(c). Auger survey scans show the concentrations of Sm, Ga, and O to be 54.2%, 3.1%, and 42.7% respectively. The Ga and O concentration show a sharp increase at 55 cycles of the depth profile with a cycle interval of 0.20 min/cycle (Figure 6(a)). XPS analysis of the films showed an O to Sm metal ratio roughly comparable to that obtained in films grown at 100ºC (Table 2).The RMS roughness value was 1.0 nm, representing a significant increase with substrate temperature. The TEM micrographs clearly show evidence of atomic registry at a crystalline interface (Figure 6(b). The breakdown field strength was 2.95 MV/cm and the C-V characteristics indicated a flat band voltage shift of 1V accumulation in the forward direction and depletion in the reverse direction. Since the C-V curves with this sample showed a significant ( $\geq$ 3 pF) change in capacitance as the device was swept from depletion to accumulation, hysteretic C-V curves were also collected. Measurements at 10 kHz clearly showed the hysteretic behavior of the C-V curves. The gate voltage was swept from depletion to accumulation and back to depletion.

**(e) Growth and Characterization of Bi-Layer $(Sm_xGa_{1-x})_2O_3$ Oxide Stack**

A dielectric layer with high breakdown field is desirable from an electrical standpoint allowing for the growth of thinner oxides with less leakage [2,39]. Polycrystalline oxide films deposited at low substrate temperatures typically produce better breakdown behavior than more textured or single crystal films deposited at higher substrate temperatures. Conversely, the crystalline interfaces obtained at the higher substrate temperatures typically produce lower interface state densities.

One method of combining the best characteristics of both of these microstructures is to grow the interfacial oxide layer at a high temperature and then drop the temperature for the remainder of the layer. Such a bi-layer oxide stack was grown to combine the interfacial properties of oxide growth at 500ºC and the high breakdown field and surface morphology properties of oxide growth at 100ºC. The oxide film grown at 100ºC exhibited an amorphous nature with breakdown field strength of 3.63 MV/cm and rms value of 0.4 nm. Films grown at 500ºC were crystalline at the interface with a breakdown field strength of 2.95 MV/cm. A flat band voltage shift of 1 V for the oxide film grown at 500ºC is an indication of smaller fixed oxide charge and the C-V characteristics clearly showed accumulation and depletion.

The growth procedure used for the growth of each layer was identical the only difference being the substrate temperature. The growth of the bi-layer oxide stack began with a substrate temperature of 500ºC. The substrate temperature remained at 500ºC for 7.5 minutes. The substrate was rotated away from the sources and cooled to 100ºC. The sample was then rotated back into the growth position for the remainder of the growth run. The powder XRD measurements of the bi-layer stack showed the presence of the cubic phase at 30.01º associated with $Sm_2O_3$ (321) orientation. The remaining peaks in the spectrum were identified as GaAs peaks. The surface morphology was relatively smooth with an RMS roughness value of 0.5 nm. The breakdown field was measured at 3.13 MV/cm (Figure 7(a). The C-V characteristics of the bi-layer oxide were extremely noisy and thus a $D_{it}$ measurement could not be determined.

**(f) Annealing Study of Sm-Based Oxides**

Annealing in oxygen was attempted to oxidize residual Sm metal in the oxide layer revealed by XPS measurements. $Sm_2O_3$ and $(Sm_xGa_{1-x})_2O_3$ samples were annealed at 500ºC for thirty minutes while being exposed to the oxygen plasma. The ratio of intensities of the oxidized metal peak to the Sm free metal peak increased while the ratio of the intensities of the Sm free metal

peak to the oxidized metal peak decreased as a result of post-growth annealing in oxygen of $Sm_2O_3$ films (Table 3). XRD measurements were taken of sample grown at a substrate temperature of 500ºC before and after annealing at 500ºC for 30 minutes under an O plasma. The crystal quality degraded as a result of annealing with no change in phase distribution. After post-growth annealing in O, the RMS roughness value increased from 1.4 nm to 1.6 nm and 0.6 nm to 0.7 nm for $Sm_2O_3$ on GaAs grown at substrate temperature of 100ºC and 500ºC respectively. The sharp peak around 28º degrees is an artifact due to the polychromatic nature of the x-ray source. The annealing under an oxygen plasma in the MBE system did not significantly change either the Dit or breakdown voltage.

The post-growth annealing of $(Sm_xGa_{1-x})_2O_3$ films resulted in an increase in the oxygen to metal ratio but effected no change in the crystalline phase distribution (Figure 7(b) and Table S1). The breakdown field was increased from 2.95 MV/cm to 3.37 MV/cm which is consistent with the increase in the oxygen to metal ratio and it seems to indicate a more insulating film as a result of the post-growth annealing. XRD measurements were taken of a sample grown at a substrate temperature of 500ºC and a Sm cell temperature of 550ºC before and after annealing at 500ºC for 30 minutes under an O plasma, as shown in Figure 7(b). The phase distribution was not affected but the crystal quality of the film was degraded as a result of post-growth annealing in oxygen. The RMS roughness value increased from 1.0 nm to 1.5 nm for $(Sm_xGa_{1-x})_2O_3$ on GaAs grown at a substrate temperature of 500ºC.

We also conducted Rapid Thermal Annealing (RTA) of $(Sm_xGa_{1-x})_2O_3$ films under forming gas at 300ºC for 45 seconds. Annealing in a reducing atmosphere should create more dangling bonds by reacting with the oxygen and should result in an increase in the metal to oxygen ratio (Table S2). The metal to oxygen ratio increased from 0.161 to 0.249. The hysteretic C-V characteristics taken at 10 kHz was measured and compared to the hysteretic C-V curve taken at 10kHz before annealing in

forming gas. Since it was determined that annealing in forming gas results in a film with more unbonded metal, $Sm_2O_3$ films were not annealed in forming gas.

Post-growth annealing under an oxygen plasma in the MBE system was successful in oxidizing some of the unbonded Sm metal. However, it was not successful in changing the phase composition from a mixture of monoclinic and cubic oxide to one of pure cubic phase. Annealing in an RTA under forming gas did not improve the electrical properties of the material and in fact increased the amount of unbonded Sm metal in the oxide. The leakage current as a function of the breakdown field was compared for films grown under all growth conditions (Figure 8(a). It was determined that the binary oxide grown at 100ºC exhibited the best electrical properties in terms of breakdown field. Ternary oxides grown at 500ºC showed the best CV behavior, displayed in Figure 8(b).

**CONCLUSIONS**

$Sm_2O_3$ metal-modulated growth at a high temperature (500ºC) produced single crystal films, while growth at low temperature (100ºC) yielded amorphous films. $Sm_2O_3$/GaAs diodes show good breakdown fields (3.9 MV/cm) with relatively low $D_{it}$. Growth of the ternary $(Sm_xGa_{1-x})_2O_3$ at 500ºC produced polycrystalline films with a crystalline interfacial layer of approximately 65 Å. Some evidence of Ga segregation at the interface was observed with AES depth profiling. Similar growth at 100°C produced films which were amorphous. A significant amount of Sm free metal was also observed in all of these films. Despite this, breakdown fields up to 4.35 MV/cm were achieved. Higher growth temperatures produced better CV behavior. Overall, however, the best leakage currents were obtained in the pure $Sm_2O_3$. Future work could include growth of a digital alloy, which has proven successful for growth of $(Sc_xGa_{1-x})_2O_3$ alloys [39].

Future work on this material system should also focus on further reducing the unbonded metal in the oxide which should lead to improved electrical behavior. In its present form, the oxide should be adequate for use as a field plate but needs further optimization to be useful as a gate dielectric.

**ACKNOWLEDGMENTS**

The authors would like to thank the Research Service Center (RSC) staff at the University of Florida for their help in the fabrication and characterization of these materials. The work was performed as part of Interaction of Ionizing Radiation with Matter University Research Alliance (IIRM-URA), sponsored by the Department of the Defense, Defense Threat Reduction Agency under Award No. HDTRA1-20-2-0002. The content of the information does not necessarily reflect the position or the policy of the federal government, and no official endorsement should be inferred. The work was also supported by the NSF [No. DMR 1856662 (James Edgar)].

**AUTHOR DECLARATIONS**

**Conflict of Interest**

The authors have no conflicts to disclose.

**DATA AVAILABILITY**

The data that support the findings of this study are available within the article

**REFERENCES**

1. C. Convertino, C.B. Zota, H. Schmid, D. Caimi, L. Czornomaz, A. Ionescu and K.E. Moselund, Nat. Electron. **4,** 162 (2021).

2. B.P. Gila, F. Ren, C.R. Abernathy, Mater. Sci. Eng. R **44**, 151 (2004).

3. L. S. Wang, L. Liu, J. P. Xu, S. Y. Zhu, Y. Huang, and P. T. Lai, IEEE Trans. Electron Devices, **61**, 742 (2014).

4. J. Robertson and Y. Guo, "Defects and reliability of high K gate stacks on Si, Ge and III–Vs," 2016 13th IEEE International Conference on Solid-State and Integrated Circuit Technology (ICSICT), 2016, pp. 495-498, doi: 10.1109/ICSICT.2016.7998961

5. A. Jönsson, J. Svensson, L.A. Wernersson, IEEE Electron Device Lett. **39**, 935 (2018).

6. O. Kilpi, M. Hellenbrand, J. Svensson, A.R. Persson, R. Wallenberg, E. Lind and L. Wernersson, IEEE Electron Device Lett. **41**, 1161 (2020).

7. Kaveh Ahadi and Ken Cadien, J. Vac. Sci. Technol A **39**, 032407 (2021).

8. S.H. Kim, I. Roh, J.H. Han, D.M. Geum, S.K. Kim, S. S. Kang, H.K. Kang, W.C. Lee, S.K. Kim and D.K. Hwang, IEEE J. Electron Devices Soc. **9**, 42 (2021).

9. Chandreswar Mahata, Mullapudi V. Jyothirmai, Mahesh Kumar Ravva, Sabyasachi Chakrabortty, Sungjun Kim, Sajal Biring, Seeram Ramakrishna, Goutam Kumar Dalapati, J. Alloys Comp., **910**, 164817 (2022).

10. Zhongyunshen Zhu, Adam Jönsson, Yen-Po Liu, Johannes Svensson, Rainer Timm and Lars-Erik Wernersson, ACS Appl. Electron. Mater., **4**, 531 (2022).

11. S. Kundu, T. Shripathi, and P. Banerji, Solid State Commun., **151**, 1881 (2011).

12. M. Saravanan, Eswaran Parthasarathy, Microelectron J., **114**, 105102 (2021).

13. Lin Hao, Gang He, Shanshan Jiang, Zhenxiang Dai, Ganhong Zheng, Jinyu Lu, Lesheng Qiao, Jingbiao Cui, J. Mater. Sci. Technol,**121**, 130 (2022).

14. W. Lu, I.P. Roh, D. Geum, S. Kim, J.D. Song, L. Kong and J.A. Alamo, 10-nm Fin-Width InGaSb p-Channel Self-Aligned FinFETs Using Antimonide-Compatible Digital Etch, 2017 IEEE International Electron Devices Meeting (IEDM); IEEE, 2017; pp 17.17.11– 17.17.14.

15. J. H. Yum, T. Akyol, D. A. Ferrer, J. C. Lee, S. K. Banerjee, M. Lei, M. Downer, T. W. Hundall, C. W. Bielawski, and G. Gersuker, J. Vac. Sci. Technol. B, 29, 061501 (2011).

16. D'Acunto, G.; Troian, A.; Kokkonen, E.; Rehman, F.; Liu, Y.-P.; Yngman, S.; Yong, Joachim Schnadt and Rainer Timm, ACS Appl. Electron. Mater. **2020**, 3915 (2020).

17. Avijit Dalal, Shyam Murli Manohar Dhar Dwivedi, Chiranjib Ghosh, Rini Lahiri, Mohamed Henini, Aniruddha Mondal, J. Alloy Comp, **868**, 159178 (2021).

18. L. S. Wang, J. P. Xu, L. Liu, W. M. Tang, and P. T. Lai, Appl. Phys. Exp. **7**, 061201 (2014).

19. H. H. Lu, J. P. Xu, and L. Liu, IEEE Trans. Device Mater. Reliab. **16**, 617 (2016).

20. H. H. Lu, L. Liu, J. P. Xu, P. T. Lai, and W. M. Tang, IEEE Trans. Electron Devices, **64**, 1535 (2017).

21. H. H. Lu, J. P. Xu, L. Liu, P. T. Lai, and W. M. Tang, IEEE Trans. Electron Devices, **64**, 2179 (2017).

22. J. Robertson and B. Falabretti, J. Appl. Phys **100**, 014111 (2006).

23. Igor Krylov, Dan Ritter and Moshe Eizenberg, Appl. Phys. Lett. **107**, 103503 (2015).

24. Igor Krylov, Dan Ritter and Moshe Eizenberg, J. Appl. Phys. **122**, 034505 (2017).

25. Y. Guo, H. Li and J. Robertson, J. Appl. Phys. **119**, 204101 (2016)

26. S. Yoshida, D. Lin, A. Vais, A. Alian, J. Franco, S. El Kazzi, Y. Mols, Y. Miyanami, M. Nakazawa, N. Collaert, H. Watanabe and A. Thean, Appl. Phys. Lett. **109**, 172101 (2016).

27. Vamsi Putcha, Jacopo Franco, Abhitosh Vais, Ben Kaczer, Qi Xie, Jan Willem Maes, Fu Tang, Michael Givens, Nadine Collaert, Dimitri Linten, Guido Groeseneken, Microelectron. Rel.,**115**, 113996 (2020).

28. F.H. Chen, M.N. Hung, J. F. Yang, S.Y. Kuo, J. L. Her, Y.H. Matsuda and T.M. Pan, J. Phys. Chem. Solids, **74**, 570 (2013).

29. W.C. Chin, K.Y. Cheong and Z. Hassan, Mat. Sci. Semicond. Proc, **13**, 303 (2010).

30. S.Y. Huang, T.C. Chang, M.C. Chen, S.C. Chen, H.P. Lo, H. C. Huang and M.J. Tsai, State Electron, **63**, 189 (2011).

31. S. Kaya, E. Yilmaz, H. Karacali, A.O. Cetinkaya and A. Aktag, Mater. Sci Semicond., **33**, 42 (2015).

32. C. Constantinescu, V. Ion, A.C. Galca and M. Dinescu, Thin Solid Films, **520**, 6393 (2012).

33. A. D. Stewart, A. Gerger, B. P. Gila, C. R. Abernathy and S. J. Pearton, Appl. Phys. Lett. **92**, 153511 (2008).

34. N. Isomura, S. Tsukamato, K. Iizuka, Y. Arakawa, J. Cryst. Growth **301/302**, 26 (2007).

35. M. Hong, J. Kwo, A.R. Kortan, J.P. Mannaerts, A.M. Sergent, Science 283, 1897 (1999).

36. M. Hong, M. Passlack, J.P. Mannaerts, J. Kwo, S.N.G. Chu, N. Monya, S.Y. Hou, V.J. Fratello, J. Vac. Sci. Technol. B**14**, 2297 (1996).

37. J.-J. Chen, B.P. Gila, M. Hlad, A. Gerger, F. Ren, C.R. Abernathy, S.J. Pearton, Appl Phys Lett **88**, 042113 (2006).

38. Anthony D. Stewart, Andrew G. Scheuermann, Andy P. Gerger, Brent P. Gila, Cammy R. Abernathy and Stephen J. Pearton, MRS Online Proceedings Library 1108, 1003 (2008). https://doi.org/10.1557/PROC-1108-A10-03

39. Mark S. Hlad, Brent P. Gila, Cammy R. Abernathy, Fan Ren, and S. J. Pearton, J. Vac. Sci. Technol A **40**, 043403 (2022).

Table 1. List of $(Sm_xGa_{1-x})_2O_3$ films grown with different Sm cell temperatures showing the oxide, metal, and oxygen XPS peak intensities, ratio of XPS peak intensities and breakdown field. The substrate temperature was 100ºC for all samples.

| Sm cell temp (ºC) | Oxide peak counts | Sm metal peak counts | O peak counts | Ratio metal-oxidized metal counts | Breakdown field (MV/cm) |
|---|---|---|---|---|---|
| 510 | 42,011 | 6830 | 9150 | 0.16 | 4.35 |
| 530 | 41,386 | 7373 | 8161 | 0.18 | 3.11 |
| 550 | 30,467 | 5635 | 6904 | 0.19 | 3.63 |
| 570 | 23,907 | 9599 | 5759 | 0.40 | 0.11 |

Table 2. $(Sm_xGa_{1-x})_2O_3$ films grown with different substrate temperatures showing oxide, metal, and oxygen XPS peak intensities, ratio of XPS peak intensities, breakdown field, and RMS roughness.

| $T_s$ (°C) | Intensity of oxide peak (counts) | Intensity of Sm metal peak (counts) | Intensity of oxygen peak (counts) | Ratio of peak intensities (metal: oxidized metal) | Ratio of peak intensities (O:Sm metal) | Breakdown field (MV/cm) | RMS (nm) |
|---|---|---|---|---|---|---|---|
| 100 | 30,467 | 5635 | 6904 | 0.19 | 0.19 | 3.63 | 0.4 |
| 300 | 38,376 | 6490 | 8606 | 01.7 | 0.19 | 3.68 | 0.7 |
| 500 | 25 | 5905 | 7532 | 0.18 | 0.19 | 2.95 | 1.0 |

Table 3. XPS peak intensities and their ratios for a $Sm_2O_3$ film grown at a substrate temperature of 100 ºC and 500ºC and a Sm cell temperature of 550ºC before and after annealing in oxygen.

| Ts (°C) | Ratio of peak intensities (metal; oxidized metal) before annealing | Ratio of peak intensities (oxidized metal: oxygen) before annealing | Ratio of peak intensities (metal: oxidized metal) after annealing | Ratio of peak intensities (oxidized metal: oxygen) After annealing |
|---|---|---|---|---|
| 100 | 0.296 | 1.643 | 0.198 | 4.08 |
| 200 | 0.191 | 2.088 | 0.128 | 4.62 |

**Figure Captions**

Figure 1. TEM micrograph of $(Sm_xGa_{1-x})_2O_3$ grown at a substrate temperature of 100ºC and a Sm cell temperature of 550ºC.

Figure 2 (a). Depth profile of $(Sm_xGa_{1-x})_2O_3$ grown at 100ºC and a Sm cell temperature of 550ºC obtained with AES. (b) Capacitance-voltage of $(Sm_xGa_{1-x})_2O_3$ grown at a substrate temperature of 100ºC and a Sm cell temperature of 550ºC. The frequency was 1 MHz.

Figure 3(a). Growth rate (blue squares, uppermost plot) and Ga concentration (orange squares, lower plot) determined by AES in $(Sm_xGa_{1-x})_2O_3$ grown at a substrate temperature of 100°C as a function of Sm cell temperature (b) breakdown voltages for diodes with $(Sm_xGa_{1-x})_2O_3$ layers grown at a substrate temperature of 100ºC as a function of Sm cell temperature.

Figure 4. AFM images of $(Sm_xGa_{1-x})_2O_3$ layer grown at a substrate temperature of 100ºC and a Sm cell temperature of 510ºC (A), 530ºC (B), 550ºC (C) 570ºC (D).

Figure 5(a). XRD scan for $(Sm_xGa_{1-x})_2O_3$ grown at a substrate temperature of 300ºC and a Sm cell temperature of 550ºC.(b) XRD scans of $(Sm_xGa_{1-x})_2O_3$ grown at Sm cell temperatures of 510ºC (top red curve) and 550ºC (middle black curve) at substrate temperature of 500ºC. The GaAs substrate scan is shown for comparison (bottom green curve).(c) XRD scans of $(Sm_xGa_{1-x})_2O_3$ grown at 500ºC (green curve), 300ºC (red curve), and 100ºC (magenta curve) substrate temperatures, respectively (beginning from the topmost curve). The Sm cell temperature was 550 ºC for all films. XRD scan of a GaAs substrate is shown for comparison (bottom black curve)

Figure 6 (a). Auger data showing spike in Ga concentration at the interface of $(Sm_xGa_{1-x})_2O_3$ grown at a substrate temperature 500ºC and a Sm cell temperature of 550ºC (b) Microstructural data of $(Sm_xGa_{1-x})_2O_3$ grown at a substrate temperature 500ºC and a Sm cell temperature of 550ºC.

Figure 7 (a). C-V measurements for a bi-layer $(Sm_xGa_{1-x})_2O_3$ oxide stack. The oxide was grown at substrate temperature of 500ºC for the first 7.5 minutes of growth and at 100ºC for the remaining 22.5 minutes of growth (b) comparison of XRD scans of $(Sm_xGa_{1-x})_2O_3$ on GaAs at a substrate temperature 500ºC and a Sm cell temperature of 550ºC before and after annealing under an $O_2$ plasma for 30 minutes at 500ºC. The as-grown plots are at bottom, the annealed at top.

Figure 8. (a) comparison of the leakage current versus the breakdown field for $Sm_2O_3$ bilayer oxide, $Sm_2O_3$ and $(Sm_xGa_{1-x})_2O_3$ at substrate temperatures of 100ºC and 500ºC.The ternary films have higher leakage and this decreases with growth temperature. The bilayer is in between the ternary and binary film results. (b) Family of C-V curves at different frequencies for $(Sm_xGa_{1-x})_2O_3$ grown at a substrate temperature of 500ºC and Sm cell temperature of 550ºC.
The capacitance increases with decreasing measurement frequency.

Journal of Vacuum Science Technology A



PLEASE CITE THIS ARTICLE AS DOI: 10.1116/6.0002135

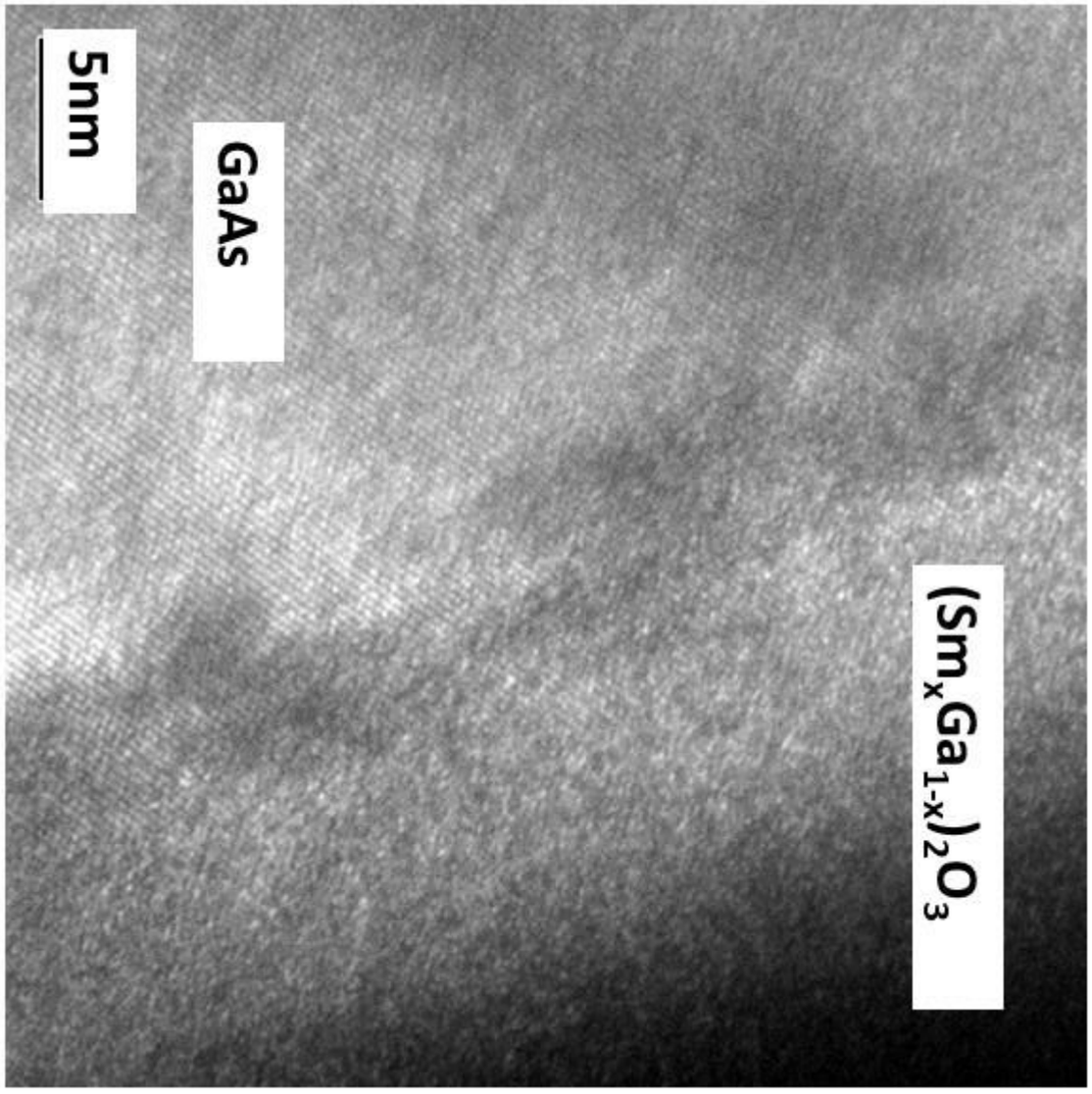

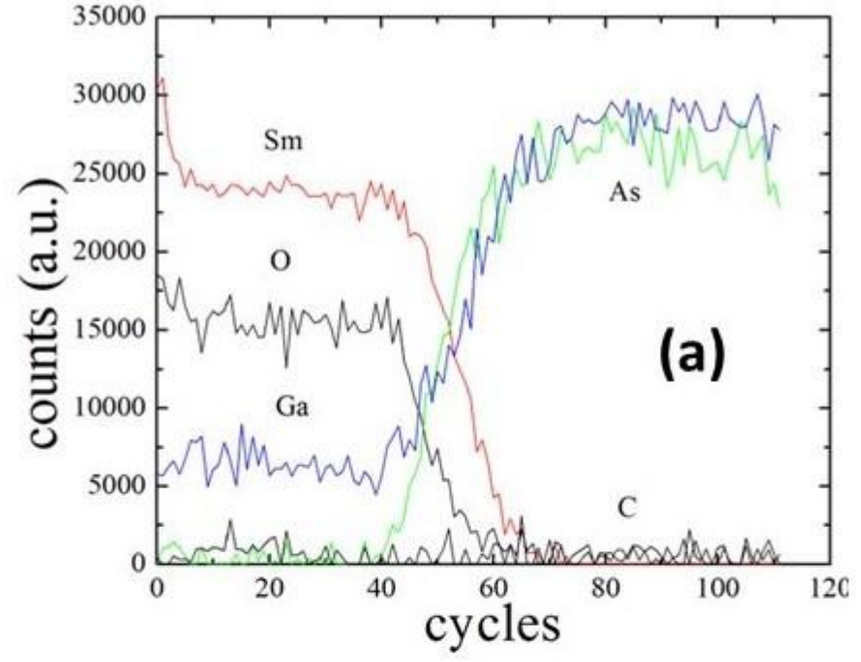


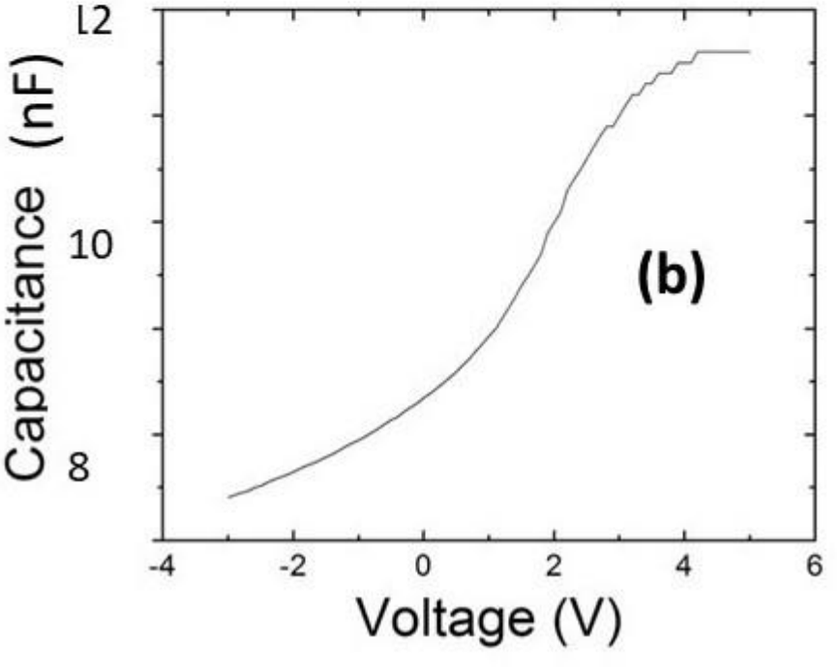

Journal of Vacuum Science Technology A


PLEASE CITE THIS ARTICLE AS DOI: 10.1116/6.0002135

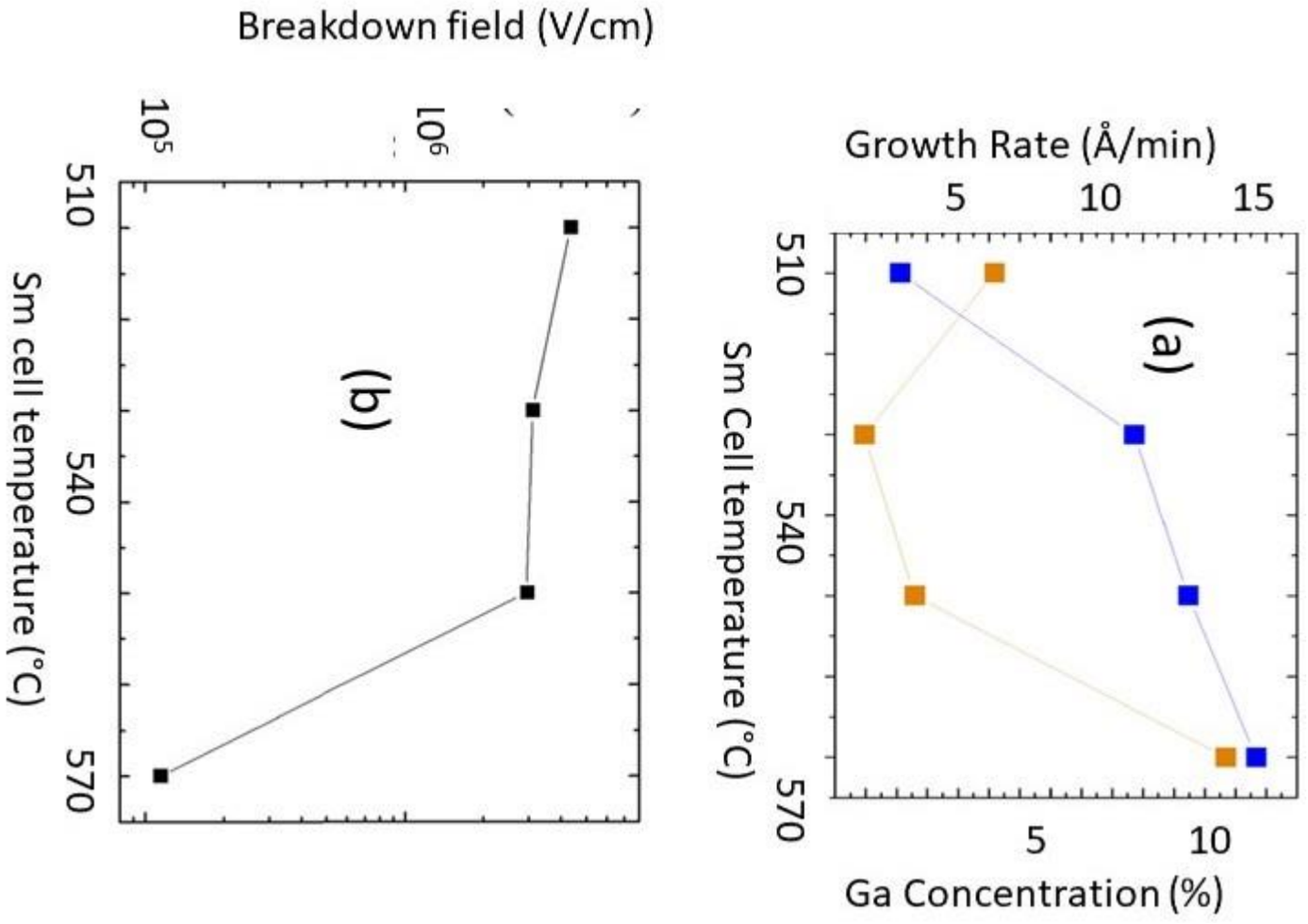

Journal of Vacuum Science Technology A


PLEASE CITE THIS ARTICLE AS DOI: 10.1116/6.0002135

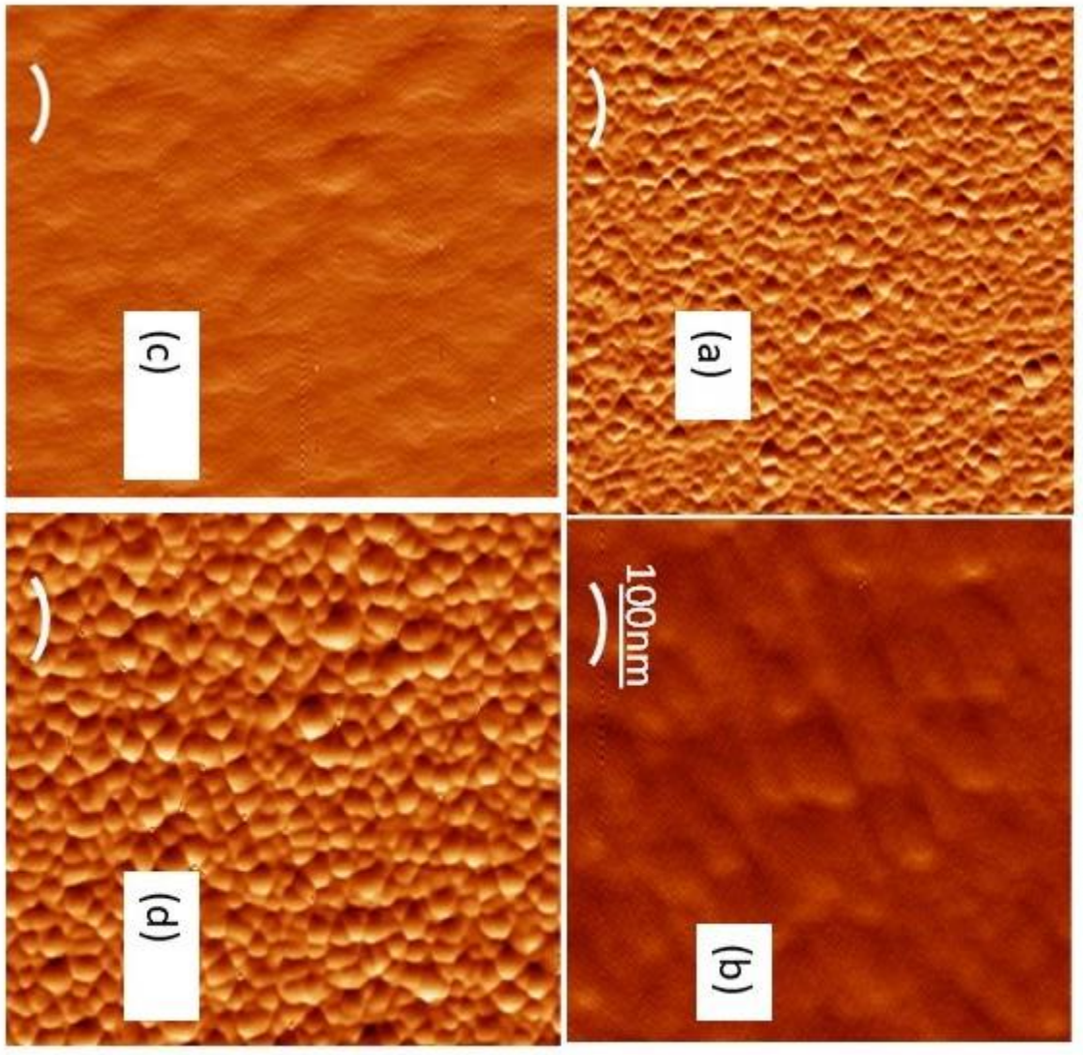

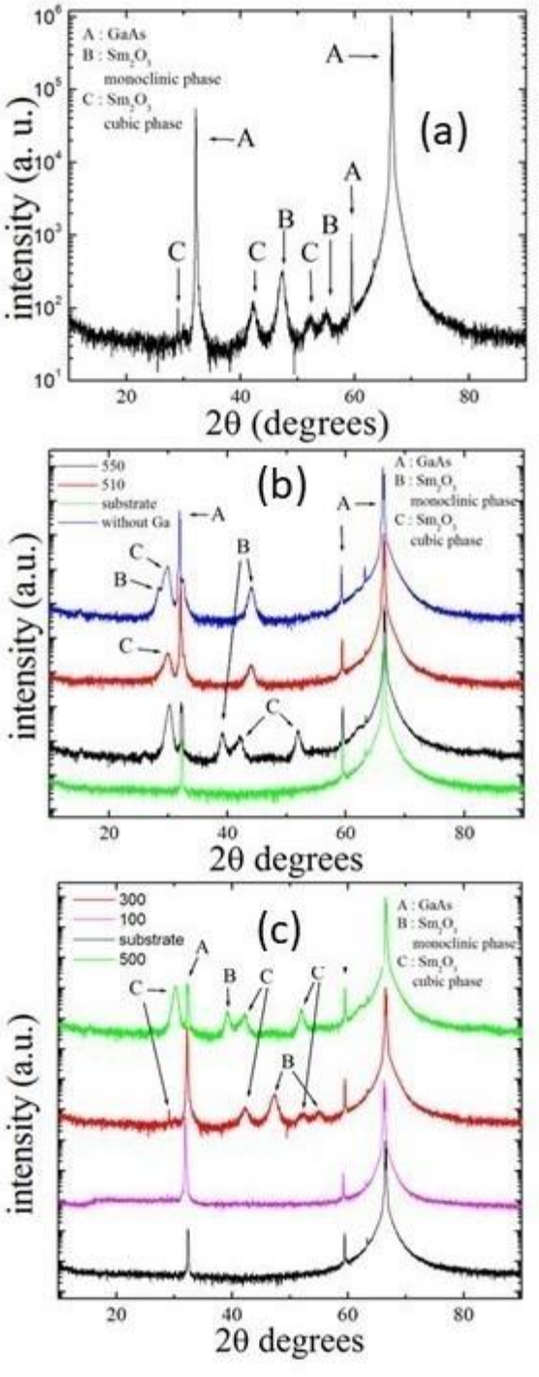

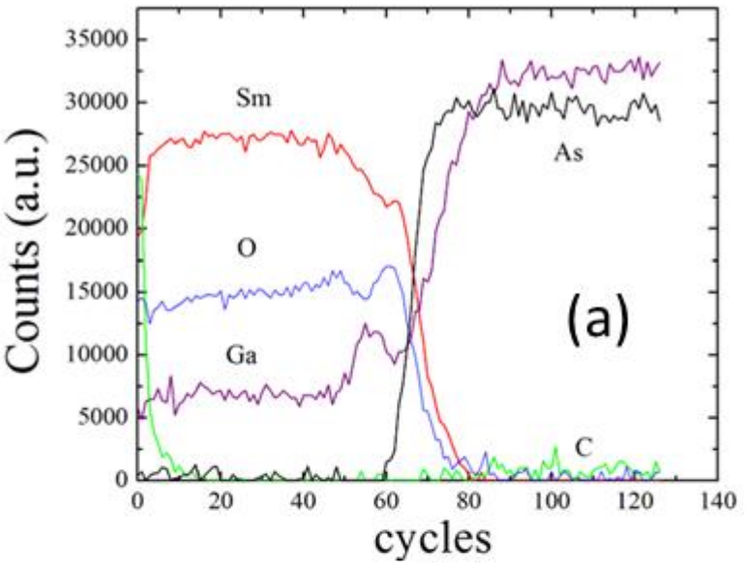


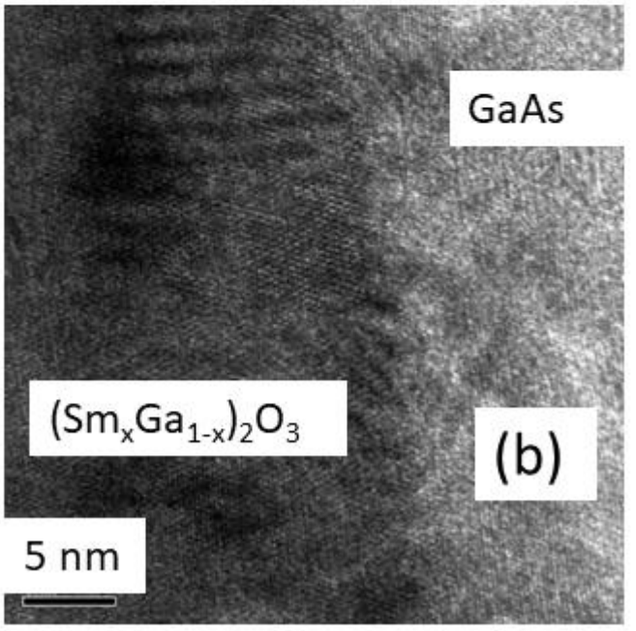

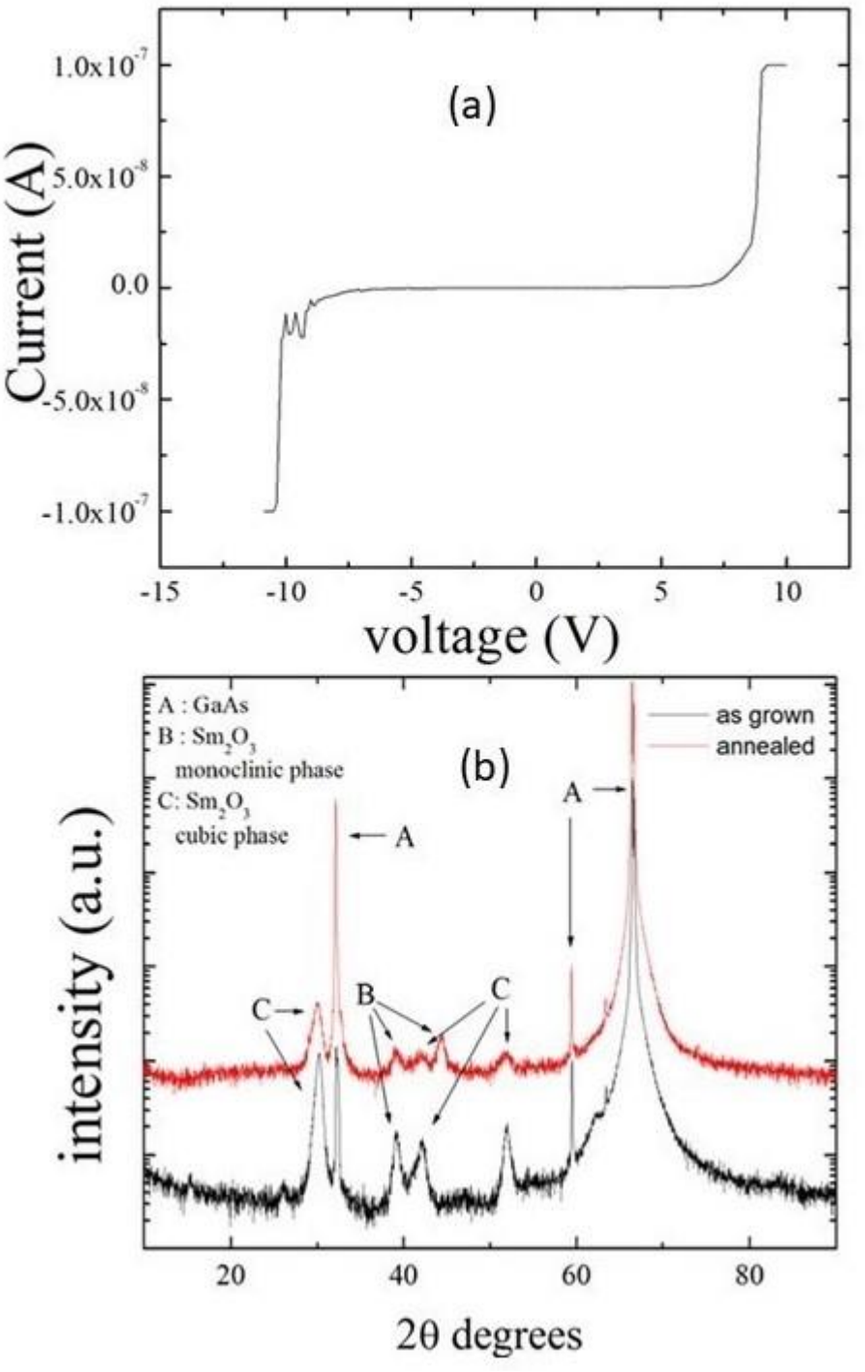

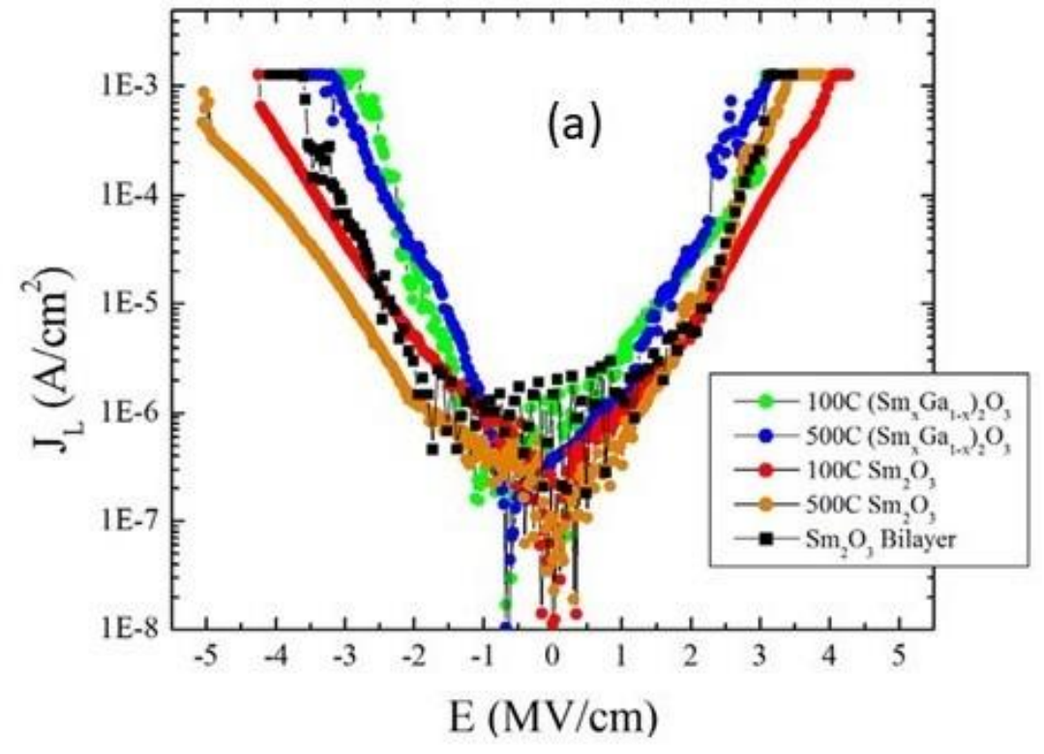


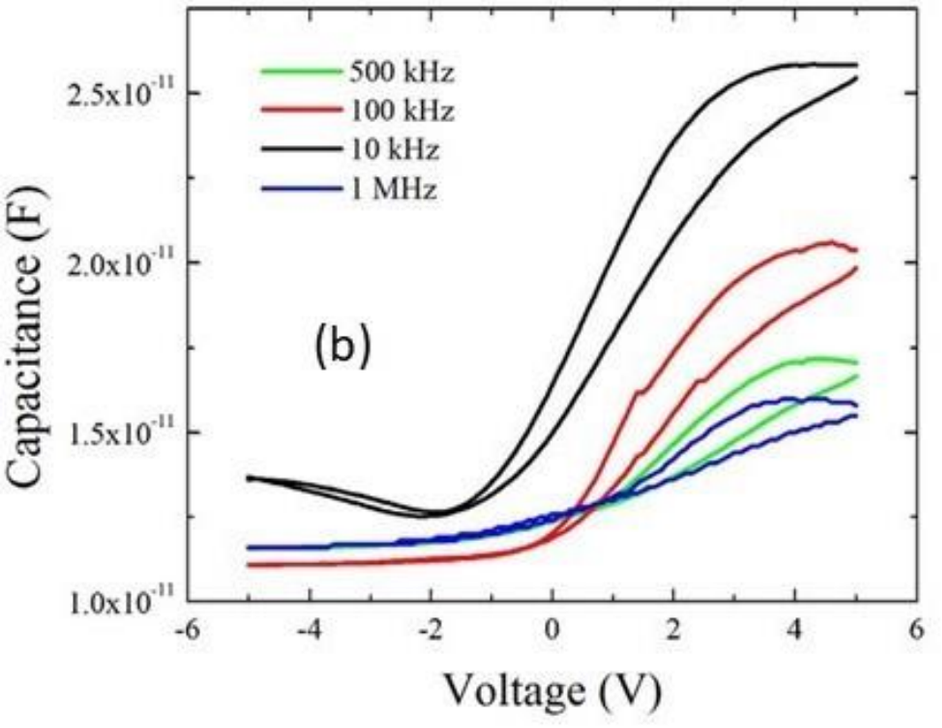

Journal of Vacuum Science Technology A

ACCEPTED MANUSCRIPT

This is the author's peer reviewed, accepted manuscript. However, the online version of record will be different from this version once it has been copyedited and typeset.
PLEASE CITE THIS ARTICLE AS DOI: 10.1116/6.0002135

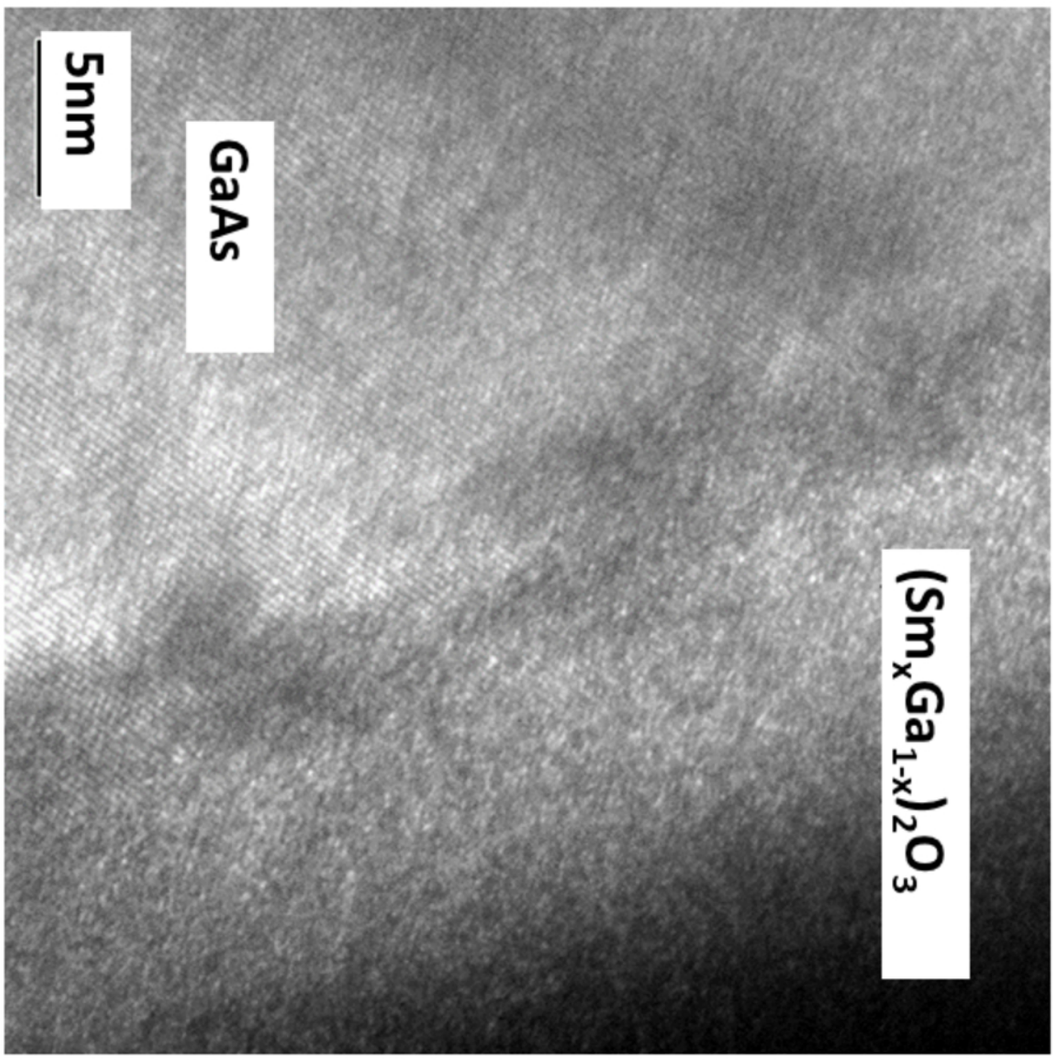

Journal of Vacuum Science Technology A

Journal of Vacuum Science Technology A



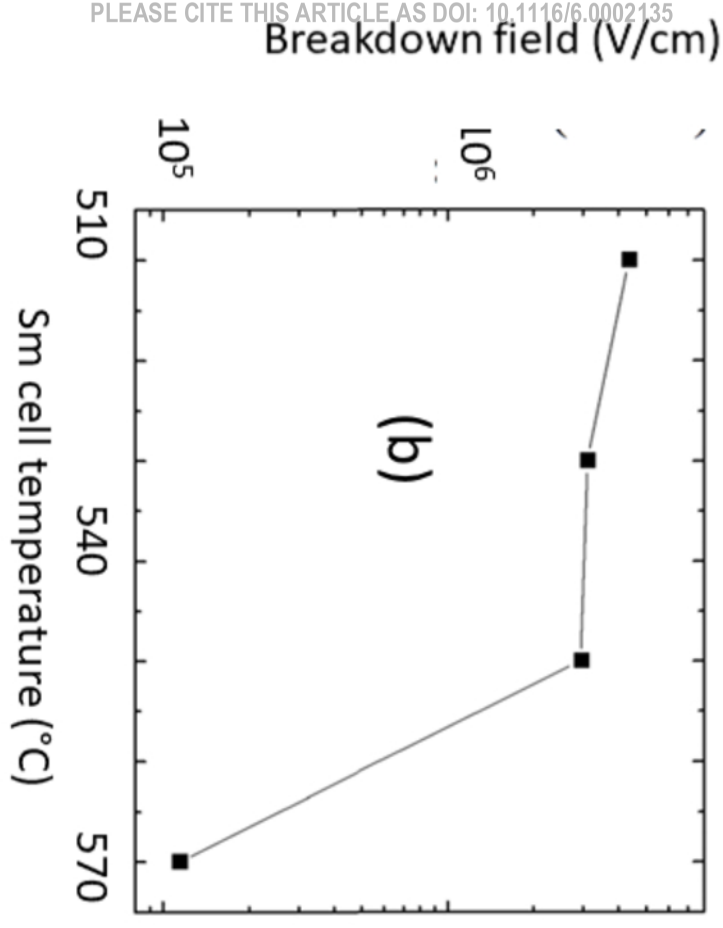


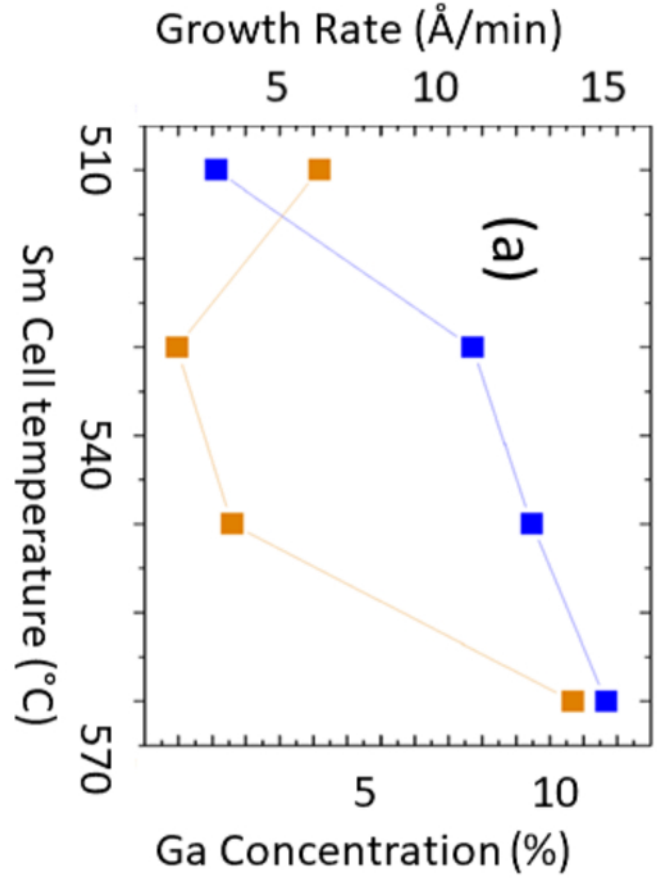

Journal of Vacuum Science Technology A

ACCEPTED MANUSCRIPT

This is the author's peer reviewed, accepted manuscript. However, the online version of record will be different from this version once it has been copyedited and typeset.
PLEASE CITE THIS ARTICLE AS DOI: 10.1116/6.0002135

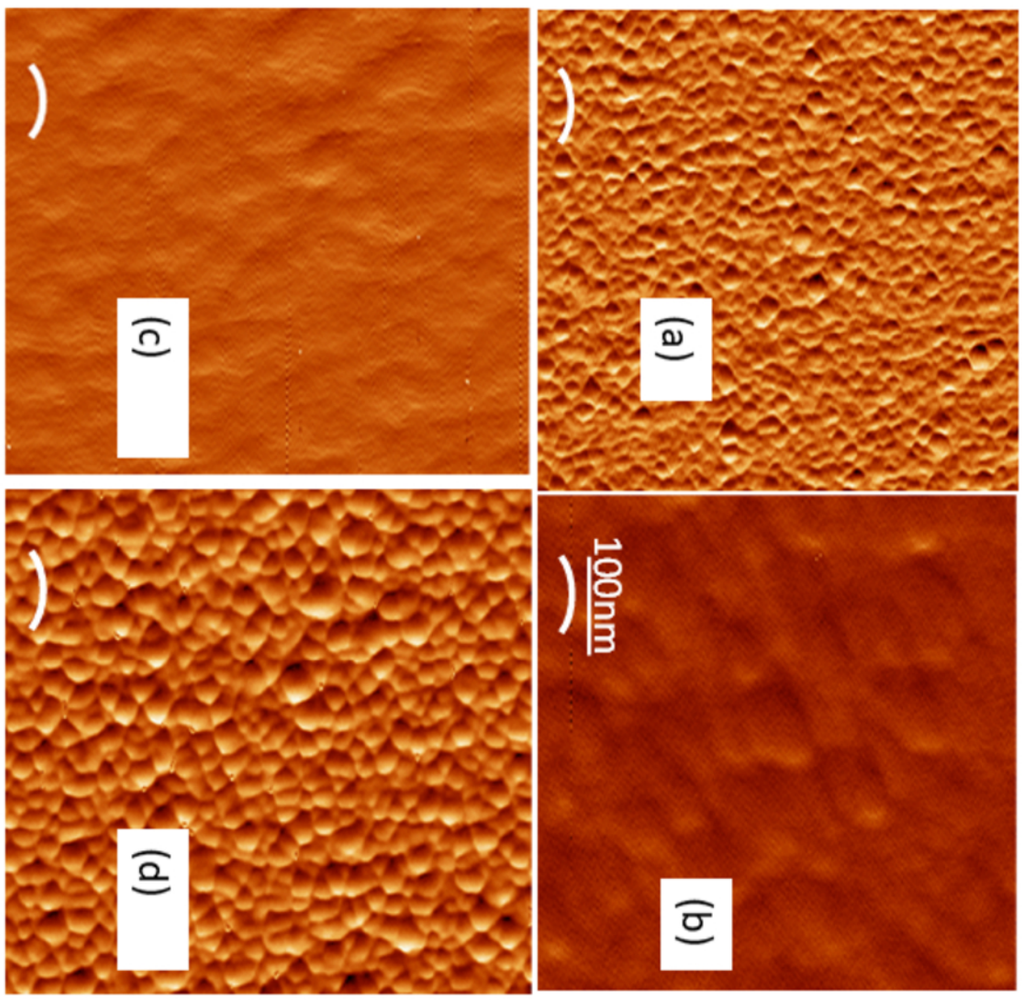

Journal of Vacuum Science Technology A



PLEASE CITE THIS ARTICLE AS DOI: 10.1116/6.0002135

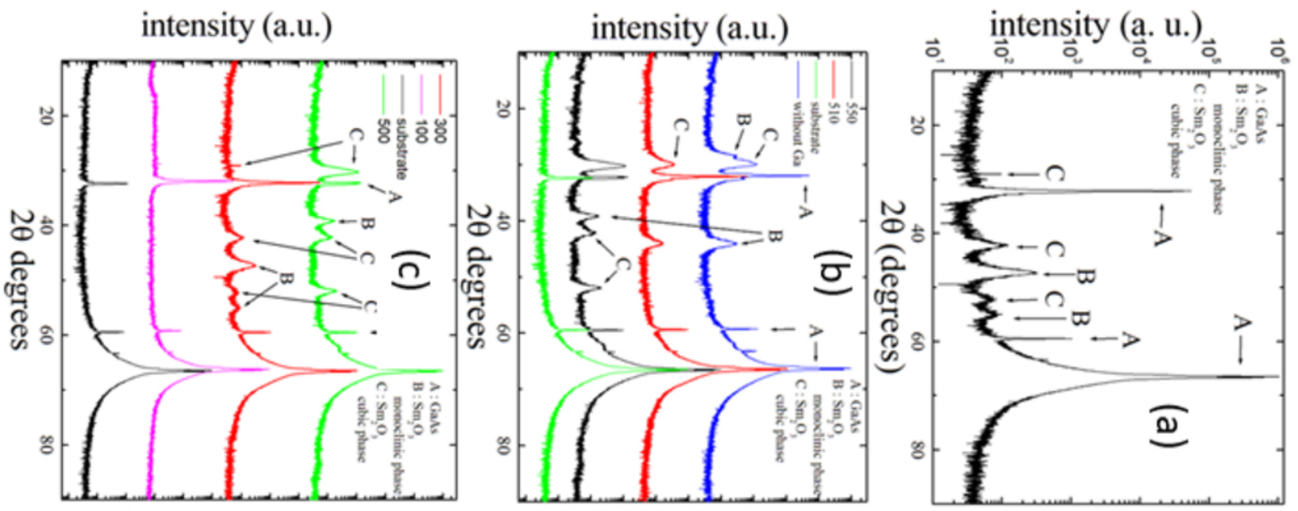

Journal of Vacuum Science Technology A



PLEASE CITE THIS ARTICLE AS DOI: 10.1116/6.0002135

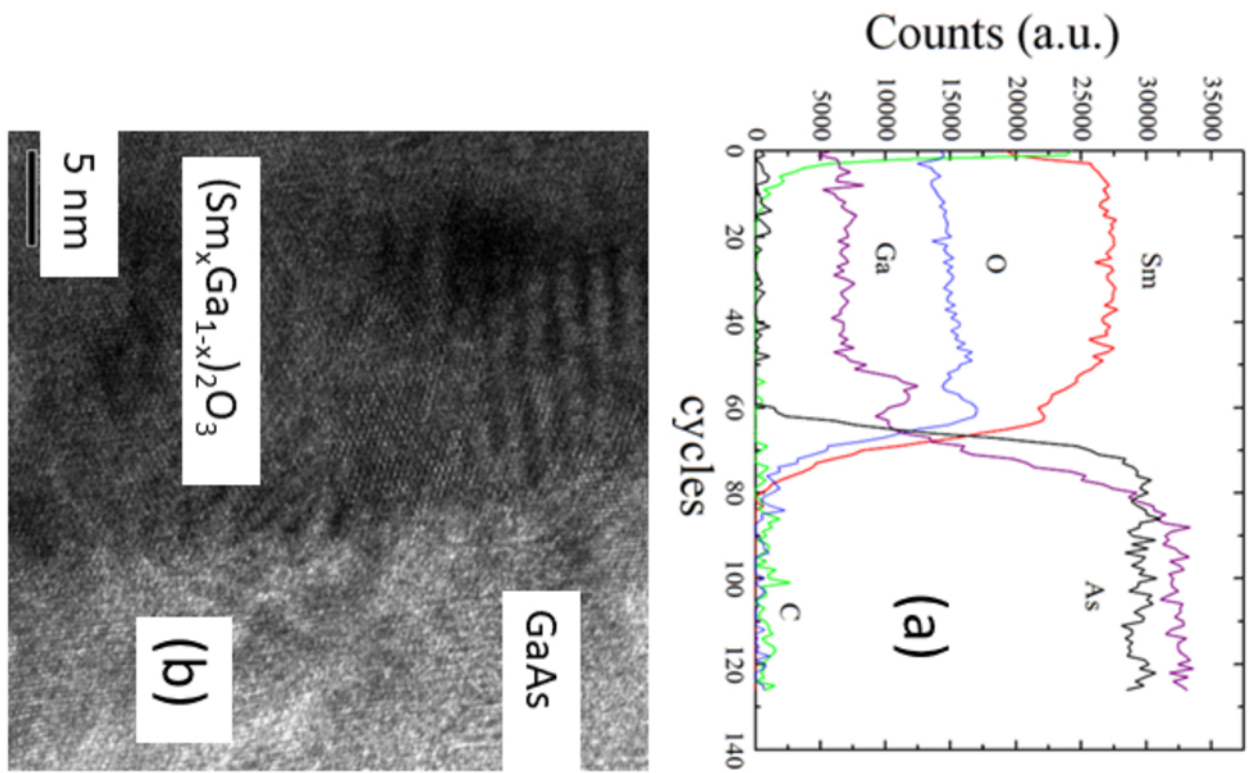

Journal of Vacuum Science Technology A



PLEASE CITE THIS ARTICLE AS DOI: 10.1116/6.0002135

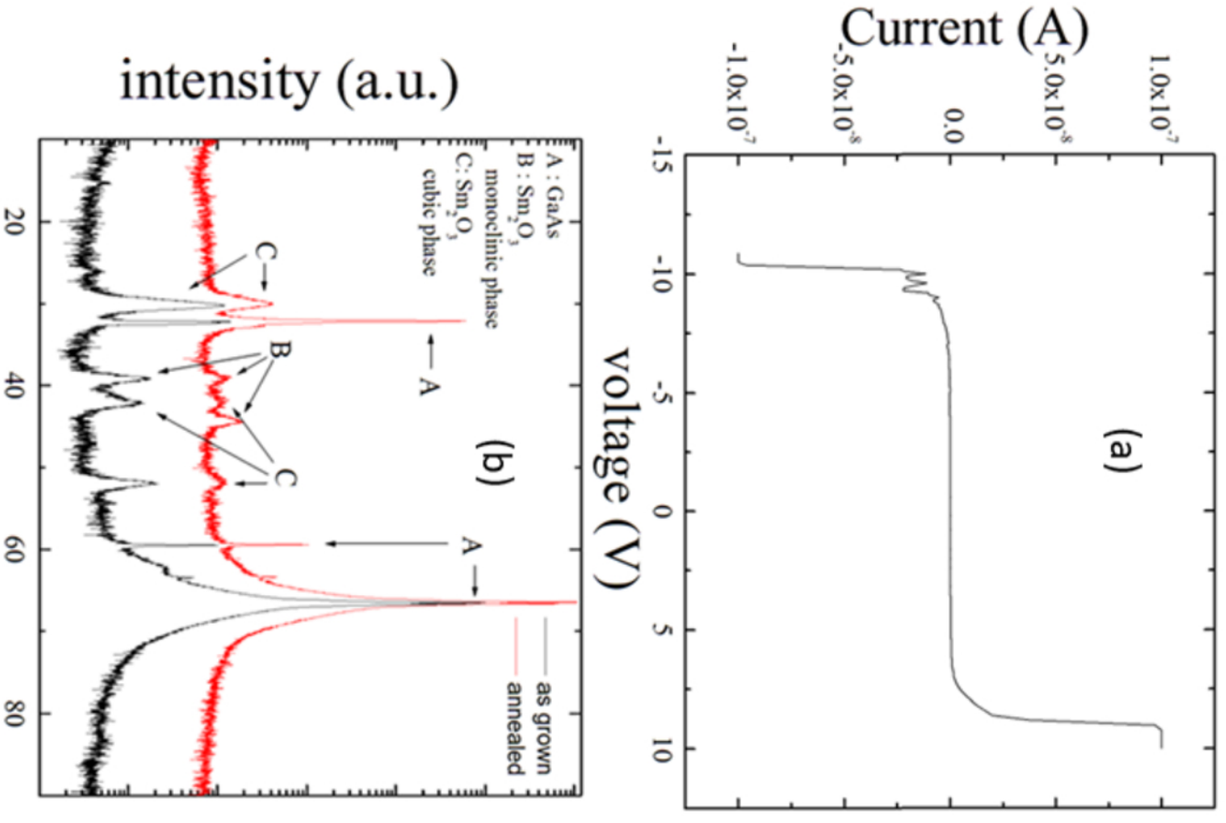

Journal of Vacuum Science Technology A



PLEASE CITE THIS ARTICLE AS DOI: 10.1116/6.0002135